



**CORRELATION OF PUMA AIRLOADS – LIFTING-LINE
AND WAKE CALCULATION**

BY

WILLIAM G. BOUSMAN
U.S. ARMY AEROFLIGHTDYNAMICS DIRECTORATE
MOFFETT FIELD, CALIFORNIA, USA

NEIL GILBERT
AERONAUTICAL RESEARCH LABORATORY
MELBOURNE, AUSTRALIA

WAYNE JOHNSON
JOHNSON AERONAUTICS
PALO ALTO, CALIFORNIA, USA

COLIN YOUNG
ROYAL AEROSPACE ESTABLISHMENT
FARNBOROUGH, ENGLAND

FRANÇOIS TOULMAY
AÉROSPATIALE
MARIGNANE, FRANCE

M. J. RILEY
ROYAL AEROSPACE ESTABLISHMENT
BEDFORD, ENGLAND

FIFTEENTH EUROPEAN ROTORCRAFT FORUM

SEPTEMBER 12 - 15, 1989 AMSTERDAM

Correlation of Puma Airloads – Lifting-Line and Wake Calculation

William G. Bousman
U.S. Army Aeroflightdynamics Directorate
Moffett Field, California, USA

Neil Gilbert
Aeronautical Research Laboratory
Melbourne, Australia

Wayne Johnson
Johnson Aeronautics
Palo Alto, California, USA

Colin Young
Royal Aerospace Establishment
Farnborough, England

François Toulmay
Aérospatiale
Marignane, France

M. J. Riley
Royal Aerospace Establishment
Bedford, England

ABSTRACT

A cooperative program undertaken by organizations in the United States, England, France, and Australia has assessed the strengths and weaknesses of four lifting-line/wake methods and three CFD methods by comparing their predictions with the data obtained in flight trials of a research Puma. The Puma has been tested in two configurations: a mixed-bladed rotor with instrumented rectangular-tip and swept-tip blades, and a configuration with four identical swept-tip blades. The present paper examines the results of the lifting-line predictions. The better lifting-line methods show good agreement with lift at the blade tip for the configuration with four swept tips; the moment is well-predicted at $.92 R$, but deteriorates outboard. The predictions for the mixed-bladed rotor configuration range from fair to good. The lift prediction is better for the swept-tip blade than for the rectangular-tip blade, but the reasons for this cannot be determined because of the unmodeled effects of the mixed-bladed rotor.

1. INTRODUCTION

Significant progress has been made in recent years in the development of computational fluid dynamic (CFD) methods for calculating the aerodynamic loads on a helicopter rotor blade in transonic flow. The development of these CFD methods has followed a logical, step-by-step process from the modeling of simplified flows to complex ones [1,2]. The first step has been to predict the flow behavior for nonlifting rotors with rigid blades where there are no flows external to the computational grid. The next step has been to examine flows for lifting rotors with rigid blades both in hover and in forward flight, and the final step has been to treat the problem of the fully aeroelastic lifting rotor in trimmed, high-speed flight. In the latter case it is necessary to account for the velocity at the blade induced by the wakes of the other rotor blades that are outside of the computational grid, as well as the velocities that are caused by blade motions. Approaches taken include modeling the external flow either by (1) using a simplified uniform inflow model or (2) coupling the analysis with a comprehensive lifting-line code that can provide not only the inflow induced by aerodynamic surfaces outside of the computational grid but also the inflow that is caused by the blade elastic response. Considerable success has been achieved using the latter approach for the prediction of the surface pressures on the SA 349/2 helicopter [3] by coupling the U.S. Army's Full-Potential Rotor (FPR) code [4] with the comprehensive model CAMRAD [5,6].

As a consequence of the rapid advancement of CFD methods, a cooperative program was undertaken by research organizations in the United States, England, France, and Australia to assess the strengths and weaknesses of the new CFD methods compared to flight test data. The objectives of this comparison were to determine in detail the predictive accuracy of these methods and to identify areas that need additional work before the methods can be successfully integrated into the helicopter design process. The approach taken was to, first, select surface-pressure and loads data obtained from flight tests of a research Puma at high advance ratio [7,8]; then employ a comprehensive lifting-line method with a vortex wake [9] to calculate the inflow at the blade; and, finally, use the calculated inflow angles as a prescribed velocity to calculate the pressures and forces with three different CFD methods [4,10,11]. The intermediate step of calculating the inflow to be used in the CFD methods is crucial to their success, so two additional comprehensive lifting-line/wake methods were added for the comparison: CAMRAD [5,6] and METAR, a new aerodynamic analysis developed at Aérospatiale.

A workshop was held at the Royal Aerospace Establishment (RAE) in Farnborough in May 1988 to compare the CFD and lifting-line/wake method predictions with flight data and to assess their strengths and limitations. The basic findings of this workshop were that the CFD methods, although they agreed well with each other, did not show good agreement with the data, while the lifting-line/wake methods did not show good agreement either with each other or with the data. The difficulties that the lifting-line/wake methods experienced in calculating the aerodynamic loads indicate that the prescribed inflow angles used in the CFD methods were not correct and, hence, the CFD predictions were not correct.

This paper and its companion paper "Correlation of Puma Airloads – Evaluation of CFD Prediction Methods" (Strawn et al., this conf.) will examine the major questions that resulted from the workshop, and summarize the substantial work that has been done subsequently. These papers address the following questions:

1. How good are the data? Are they suitable for validation purposes?
2. How well do the lifting-line/wake methods predict the airloads measured on the Puma? Can limitations in modeling capability be identified?
3. How accurate are the CFD methods for airloads prediction? Despite their dependence upon the lifting-line/wake methods for the correct modeling of the inflow, can they provide useful physical insight?
4. How satisfactory are the methods used to calculate the inflow for the CFD calculations? How important are the differences between simply prescribing the inflow (uncoupled) and iterating between the lifting-line/wake and CFD methods (coupled)?
5. Independent of the accuracy of the CFD predictions, how well do CFD methods compare with each other? What advantages are obtained as the analysis sophistication increases from the quasisteady small-disturbance theory to the unsteady small-disturbance theory to the full-potential model?

This paper will primarily address questions 1 and 2, and the companion paper will examine questions 3–5. Most of the material that is presented here is new. In addition, predictions have been made by one of us (Johnson) using CAMRAD/JA that were not part of the original comparisons. The flight test data will be discussed first, including the rationale for the cases selected. Experimental results will be shown and their importance discussed. The various lifting-line/wake methods will then be described. The lifting-line/wake method predictions

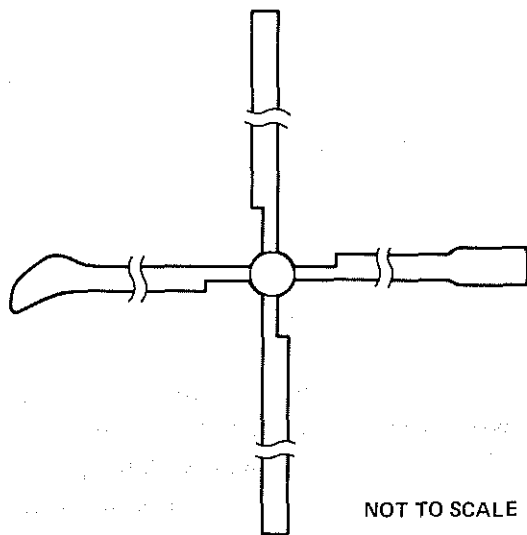


Figure 1. Mixed-bladed rotor configuration (not to scale).

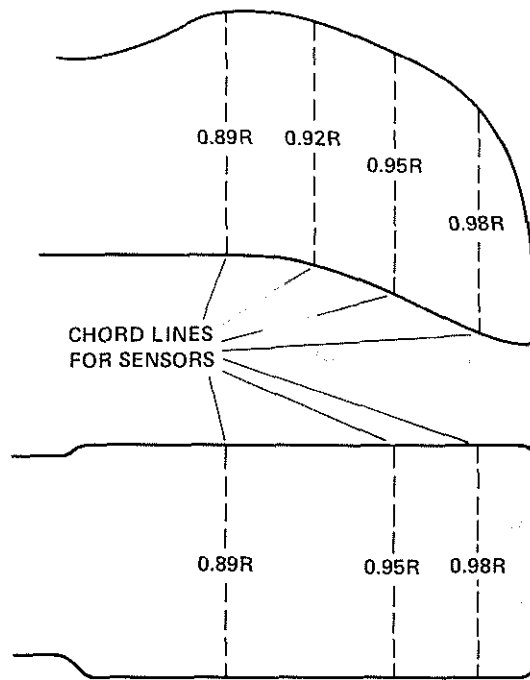


Figure 2. Pressure transducer installation on swept and rectangular tips.

will be compared to the experimental data, and known modeling limitations will be discussed. Conclusions will be made relative to the adequacy of the lifting-line/wake methods.

2. PUMA FLIGHT TEST

Puma Research Program

A series of flight experiments have been performed at the Royal Aerospace Establishment at Bedford in a collaborative program with ONERA and Aérospatiale using a Puma with modified blade tips [7,8]. The primary objective of this program was to obtain a detailed understanding of the flow around a rotor blade swept tip.

The first phase of the program examined the behavior of an instrumented swept tip by comparing it directly with an equivalent rectangular tip installed on the opposite side of the rotor. Flight conditions for the two tips were thus essentially identical. The two blades at ninety degrees to the instrumented blades were unmodified. Figure 1 shows the blade layout, and Fig. 2 shows the tip configuration. The structural provisions for the two modified blades were installed at Aérospatiale. The pressure transducers, a balsa filler, and a fiberglass skin were then added at Bedford. (Aérospatiale also built three additional swept-tip blades without pressure instrumentation for use in the second phase of the program.)

The swept tip was designed so that the center of pressure at the tip was at the elastic axis; it was important that the swept-tip blade elastic twist and pitch-link loads be similar to those of the rectangular-tip blade. The profile of the standard Puma blade is a slightly modified NACA 0012. The new tip profiles were obtained by a translation of the inboard profile as shown

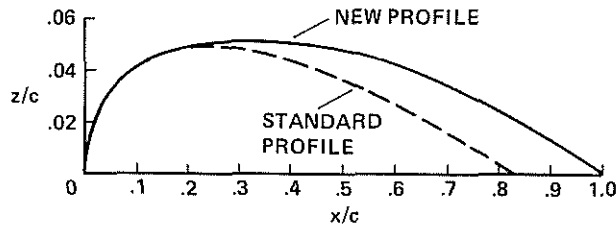


Figure 3. Profile of modified tip in relation to Puma blade section

in Fig. 3 with the upper and lower surfaces smoothed over at mid-chord. The tip profiles remain symmetric, but the thickness ratio is reduced from 12 percent to slightly over 10 percent.

Absolute pressure transducers were installed on the swept tip at four radial stations and on the rectangular tip at three radial stations (Fig. 2). The locations of these transducers relative to the local chord are given in Table 1. No pressure transducers were mounted on the lower surface at $.89 R$ on either tip. The number of pressure transducers installed on the upper surface ranged from 9 to 14, and there was good resolution near the leading edge. The number of transducers on the lower surface ranged from 5 to 7, but none were located between the leading edge and $.10 c$.

Table 1. Pressure transducer locations, x/c .

RECTANGULAR TIP						SWEPT TIP							
$.89 R$		$.95 R$		$.978 R$		$.89 R$		$.92 R$		$.95 R$		$.978 R$	
U	L	U	L	U	L	U	L	U	L	U	L	U	L
.000		.000		.000		.000		.000		.000		.000	
		.002		.002				.002		.002		.002	
.005		.005		.005		.005		.005		.005		.005	
		.010		.010				.010		.010		.010	
.020		.020		.020		.020		.020		.020		.020	
		.040		.040				.040		.040		.040	
.100		.100	.100	.100	.100	.100		.100	.100	.100	.100	.100	.100
.200		.200	.200	.200	.200	.200		.200	.200	.200	.200	.200	.200
.300		.300	.300	.300	.300	.300		.300	.300	.300	.300	.300	.300
.400		.400	.400	.400	.400	.400		.400	.400	.400	.400	.400	.400
.500		.500	.500	.500	.500	.500		.500	.500	.500	.500	.500	.500
										.700	.700	.700	.700
										.850	.850	.850	.850
1.000		1.000		1.000		1.000		1.000		1.000		1.000	

Additional measurements obtained on the rotor during the first test phase included bending and torsion moments; flap, lead-lag, and feather angles; and pitch-link loads. The normal vehicle state parameters were measured also. Data were recorded at each test point for two revolutions. The data were analyzed using the DATAMAP graphics and analysis system [12].

A second phase of flight experiments on the research Puma examined the performance and flow environment with four swept-tip blades installed. One blade was the same pressure-instrumented blade used in the first test series, and additional structural instrumentation was provided on the other blades.

Case Selection

Three cases were selected from the Puma flight test data base for the correlation studies. Rectangular-tip and swept-tip data from a single flight condition were selected for the first two cases, and data from a matching condition from the test of the four swept-tip blades was chosen as the third case. Parameters for the three cases are shown in Table 2.

Table 2. Puma Correlation Cases

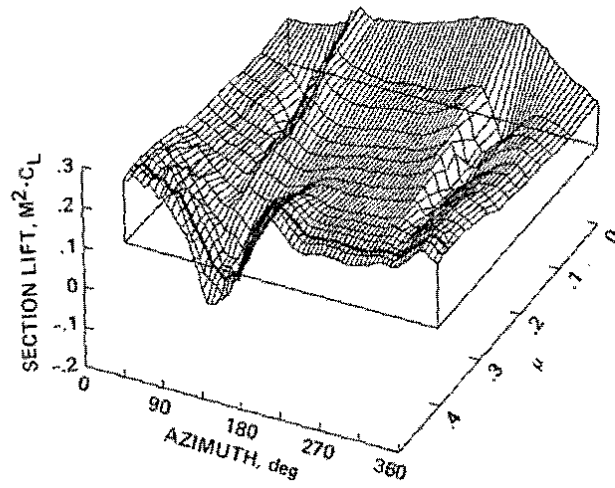
CASE	μ	C_T/σ	M_{90}	α_s	β_{1c}	β_{1s}
1	0.376	0.0798	0.857	-3.0	-0.187	0.364
2	0.376	0.0798	0.857	-3.0	-0.574	0.313
3	0.381	0.0799	0.863	-6.8	0.392	-0.074

The match in advance ratio, μ ; thrust, C_T/σ ; and advancing blade Mach number, M_{90} , is good between the two flight conditions. However, the aircraft was descending at approximately 1400 ft/min for the Case 1 and 2 flight condition, but was in level flight for the Case 3 flight condition. The different flight paths for the two conditions is indicated by the difference in shaft angle, α_s . The descent condition also causes the disk to tilt backward slightly. The rectangular-tip and swept-tip blades show a different flapping trim and therefore do not follow the same track. (Blade flapping, β_{1c} and β_{1s} , is shown as a positive Fourier series.)

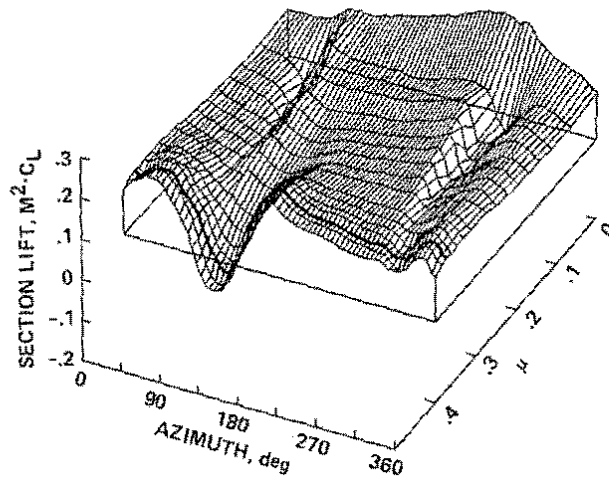
The advance ratio and thrust coefficient values were selected so that there would be extensive areas of transonic flow on the rotor, and therefore differences between the rectangular and swept tips would be evident. However, it was recognized that even at these advance ratios there would be some differences in the rotor wake because of the blade differences in the mixed-blade configuration of Cases 1 and 2. Case 3, therefore, is valuable as a control condition that can be used to separate wake effects from thrust and advance ratio effects.

Flight Test Data

The measured normal force at $.95 R$ is shown in Fig. 4 as a surface plot for the mixed-bladed rotor configuration. Measurements are shown for both the rectangular-tip and swept-tip blades. The independent variables are the advance ratio and the blade azimuth. The dependent variable is $M^2 C_L$ which is the nondimensional airload on the blade. (The multiplication by the Mach number squared, M^2 , cancels the velocity-squared term in the denominator of the lift coefficient, C_L .) This surface plot shows how the character of the flow changes as the airspeed increases. In general, both blade tips show the same variation in lift at this radial station as the advance ratio increases from zero to 0.402. In hover there is a noticeable variation in the airload around the azimuth. The unmodified blades are coned higher than the instrumented blades; their tip vortices impact the blades inboard of $.95 R$ and are the cause of some of the variation that is seen. As advance ratio is increased, the loading is dominated by the vortex of



(a) Rectangular Tip



(b) Swept Tip

Figure 4. Surface plot of measured airload at $.95R$; $C_T/\sigma = 0.08$.
 (Selected correlation cases indicated by heavy line.)

the preceding blade on both the advancing and the retreating sides of the disk. This is the well-known transition-regime vibratory loading. At $\mu = 0.25$ the vortex loading on the advancing side of the disk is no longer observed in the normal force at this radius. At higher advance ratios, the lift on the advancing side of the disk is reduced to maintain roll-moment trim, and at $\mu = 0.32$ the lift at this radius becomes negative. The cases selected for the correlation studies are shown in this figure by the heavy line.

The measured normal force and pitching moments on the blade tips are compared in Figs. 5 and 6 for the selected correlation cases. The rectangular-tip and swept-tip normal-force measurements are, in general, very similar. Both show a rapid lift reduction at the end of the first quadrant and a rapid recovery in the second quadrant. Farther out on the blade, at $.978 R$, the swept tip maintains a greater lift, which is especially noticeable over the forward portion of the disk. Both tips show an area of vortex loading at the end of the fourth quadrant. Case 3, the swept-tip control, is similar to Case 2 except that it does not show any significant loading from the preceding blade's vortex at the end of the fourth quadrant.

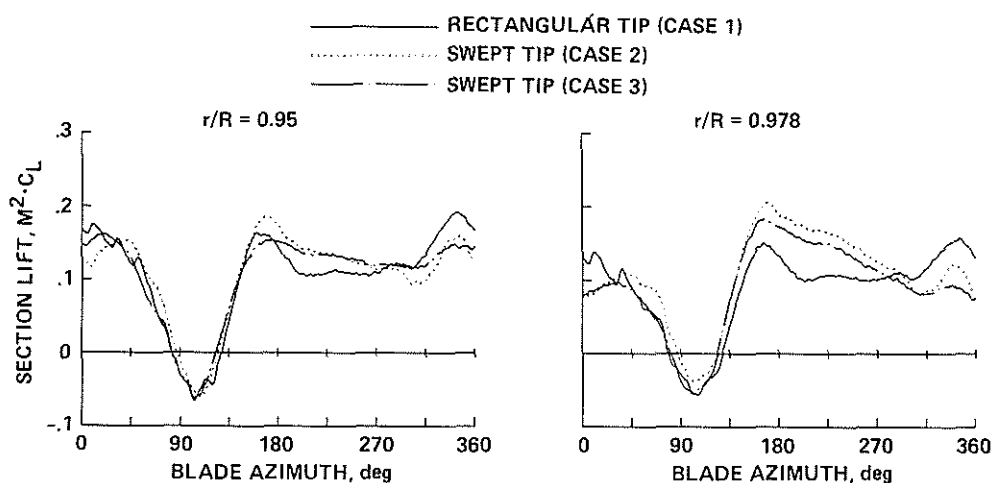


Figure 5. Comparison of normal force for Cases 1 to 3 at two radial stations.

The similarity in the measured pitching moments shown in Fig. 7 is striking. The pitching moments shown here are referred to the local quarter-chord. The three cases show similar behavior, all exhibiting a large positive moment over the first quadrant, a rapid decrease to a negative moment in the second quadrant, and then a gradual recovery in the moment over the retreating side of the disk. The rectangular-tip blade shows a more positive moment, which is more noticeable at $.978 R$. The Case 2 and 3 pitching moments agree closely.

The large pitching moments that are observed on the instrumented tips appear to be directly related to the pitch-link loads that have been measured for this flight condition. Figure 7 shows the pitch-link loads measured on the rectangular-tip, swept-tip, and unmodified blade for the Case 1 and 2 flight condition. These loads show the same positive moment in the first quadrant that was noted for the pitching moment, and then show a rapid reduction in moment to a minimum in the second quadrant. The pitch-link loads then exhibit an oscillation at 4 per rev that is not observed in the pitching-moment data at the blade tip. This oscillation appears to be a dynamic response of the control system and the blade resulting from the impressed moment variation. The alternating loads shown in Fig. 7 are more severe for the instrumented blades

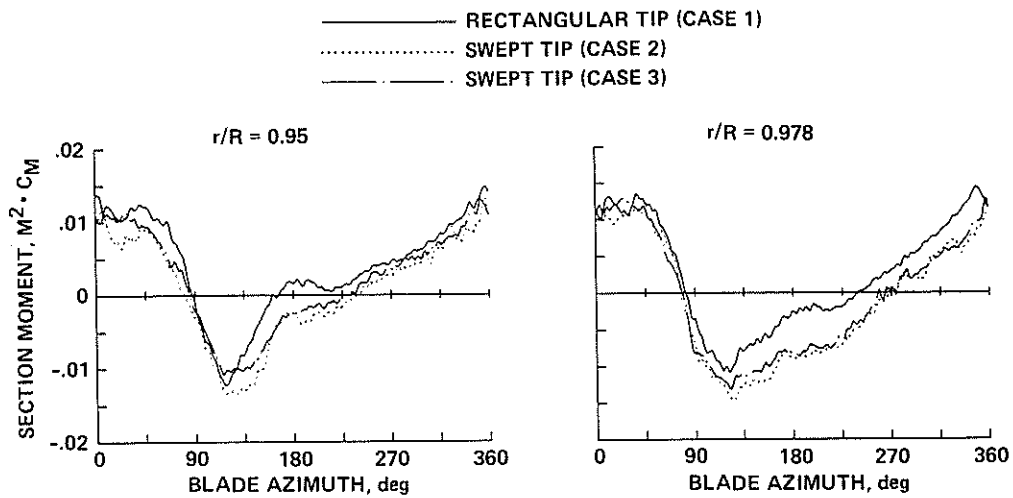


Figure 6. Comparison of pitching moment for Cases 1 to 3 at two radial stations.

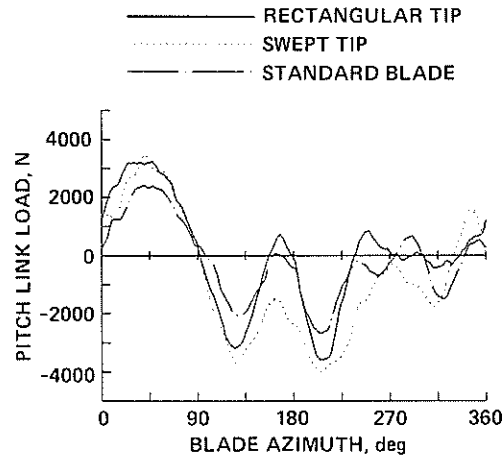


Figure 7. Measured pitch-link loads for Case 1/2 flight condition.

than for the unmodified or standard blade, but the basic character is much the same for all of these blades. The pitch-link endurance load for the Puma is approximately $\pm 2900\text{ N}$ indicating that fatigue damage is being incurred in this case for both of the instrumented blades.

Individual pressure measurements are shown in Fig. 8 for the three cases at chord locations of $.04c$ and $.10c$ at the two outer radial stations. The heavy dashed line in this figure is the critical Mach number line ($M = 1$), which is the boundary of the supercritical flow regime. Near the leading edge at $.04c$ the rectangular tip shows a large area of supercritical flow with the shock passing over the transducer in the fourth quadrant. The supercritical flow weakens in the first quadrant as the blade angle of attack is reduced. The swept tip shows only a small area of supercritical flow in the first quadrant at $.95R$ and this is weaker outboard. In the second quadrant the swept tip effect is cancelled by the radial flow and both tip planforms show comparable areas of supersonic flow. At $.10c$ the shock does not pass over the transducer location until the start of the first quadrant for the rectangular tip while the swept tip shows

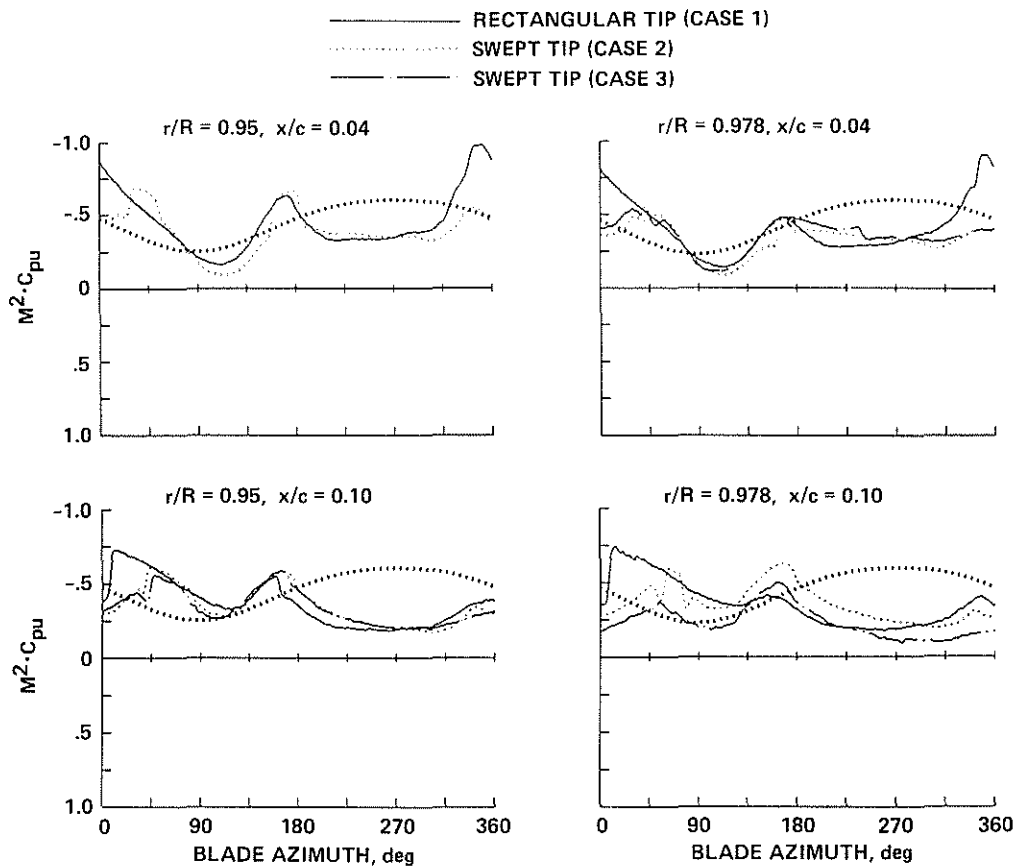


Figure 8. Comparison of measured surface pressures for correlation cases. Critical Mach number boundary shown by heavy dashed line.

a considerably reduced area of supercritical flow in this quadrant as expected. In the second quadrant the swept tip shows a greater extent of supercritical flow compared to the rectangular tip. Where there is data available for Case 3 there is good agreement with the Case 2 results. An exception is seen at $.10c$ and $.978R$ where the flow is more supercritical in both the first and second quadrants. These pressure measurements show that the detailed flow behavior over the rectangular and swept tips are quite different even though the integrated normal force and pitching moments are similar between the two tips.

3. LIFTING-LINE/WAKE METHODS

RAE/WHL Rotor Loads Program.

The RAE/WHL rotor loads program is a joint development of RAE and Westland Helicopters Ltd. based on a lifting-line analysis for the rotor aerodynamics, but formulated into a comprehensive code applicable to a wide range of rotor configurations.

The blade flexibility is modeled with a modal analysis using a maximum of eight coupled modes. The modes are calculated by a method developed at WHL by S. P. King which allows a very general blade geometry. The shear center of the blade is modeled by a series of straight-line segments that can be oriented in any direction. Secondary load paths, consisting of linear and rotational springs to earth, can be attached directly to the blade or may be positioned

at the end of a weightless arm. The root end condition may be built in or have up to three mutually perpendicular hinges, with or without restraint. The modes are usually calculated with steady loads applied which represent the blade lift and drag, thus the displacement of modes becomes a small perturbation about the steady state position.

The forced response equation is derived to a consistent order of accuracy throughout, and is fully compatible with the blade modes. There are four main forcing terms arising from the blade dynamics: the Coriolis force, the cyclic inertia force, the cyclic stiffening, and the nonlinear terms. The contributions are fairly easy to compute, as they are composed of functions of the pitch angle and its derivatives and the modal displacements, slopes, and curvatures. The Coriolis force is an inplane force resulting from the blade flapping, whereas the cyclic inertia arises from the azimuthal variations of the blade pitch. The cyclic stiffening is also caused by the pitch variation, and is composed of a series of correction terms to account for the difference between the true blade pitch and the collective pitch at which the modes are calculated. The nonlinear terms are a collection of expressions which cannot be conveniently included in any other group. The Coriolis and cyclic inertia forces are always included in the computation, but the other two terms are considered optional. For the calculations shown here the torsion terms in the cyclic stiffening and the nonlinear term were included.

The aerodynamic forcing is more difficult to calculate than are the contributions from the dynamics. The effects that must be accounted for include those of the unsteady aerodynamics, the rotor wake, the fuselage flow field, and the variation in the airfoil section properties along the span of the blade.

The aerodynamic model accounts for radial flow effects, and the aerodynamics are evaluated normal to the local quarter-chord of the blade. Section lift, drag, and moment are obtained using the stall-synthesis method of Beddoes [13] rather than from two-dimensional tables of steady section properties.

The unsteady aerodynamic effects are modeled by Wagner functions for attached flow. The dynamic stall representation uses a time delay model [13], which assumes that there are two distinct time constants which determine when the lift and pitching moment coefficients diverge once the airfoil exceeds the static angle for maximum lift.

The rotor induced velocity distribution can be calculated by one of four methods: the Glauert, the vortex ring, the vortex ring with interactive near wake, and a spiral vortex model. The development of the wake models, with the exception of the spiral vortex method, which is a recent innovation, is described by Young [9]. The vortex ring model with the interactive near wake is used in all the calculations because it represents the best compromise between accuracy and computer efficiency. Some examples of the effect of changing the wake model on the calculated blade stresses are presented in Ref. 9.

The fuselage flow field can be calculated internally in the analysis using a single source, or externally to the program using a panel method originally developed for fixed-wing aircraft. The panel method is preferred because it can give a better representation of the fuselage shape, and this method is used for the calculations presented in this paper.

The forced response equation is solved by a forward integration technique using the Z-transform. The Z-transform is similar to a Laplace transform but uses sampled rather than continuous data. Two hold circuits may be used: zero order, which assumes that the data do not change between samples; and a first-order hold, which assumes that the forcing changes linearly. The first-order hold is usually used, because it reduces the azimuth error associated with the zero-order hold.

The calculations were made using an azimuth increment of 5° . The rotor was trimmed by matching the first harmonic flapping angles, the shaft angle of attack, and the rotor thrust (assumed equal to the aircraft weight).

CAMRAD Model.

CAMRAD (Comprehensive Analytical Model of Rotorcraft Aerodynamics and Dynamics) is a comprehensive code that allows the solution of a number of problems for a wide range of rotorcraft configurations in a single, consistent analysis [5, 6, and 14]. The code was developed by Dr. W. Johnson at NASA Ames Research Center and is now used widely throughout the government and in industry in the U.S. The version used here was modified by Dr. C. Tung of the U.S. Army Aeroflightdynamics Directorate at Ames to allow the effects of the near wake to be removed to facilitate coupling with the FPR code [15]. The near wake effects are removed only when CAMRAD is used to provide a partial angle-of-attack distribution for the CFD codes.

The first step in running CAMRAD is to obtain a trim solution in which the control positions and the aircraft orientation are determined for the specified operating condition. The periodic blade motion is calculated and then the rotor performance, aerodynamic and structural loads, and rotor noise may be calculated.

The structural model of the rotor is based on engineering beam theory for rotating wings with large pitch and pretwist. A single load path is assumed and the blade is considered to have a straight, undeformed elastic axis—a recognized deficiency in modeling a swept tip. The blade motion is described by rotating, free vibration modes, equivalent to a Galerkin analysis. For the Puma correlation studies reported here, the rotor model has rigid flap and lag with four coupled flap-lag elastic bending modes, together with rigid pitch (with control-system stiffness) and one elastic torsion mode.

The rotor aerodynamic model is based on lifting-line theory, and uses steady two-dimensional airfoil characteristics provided in tables of section lift, drag, and pitching moment, defined over a grid of angle-of-attack and Mach number values. These tables are derived either from analytical expressions or from experimental data in the form of C81 tables. Analytical expressions have been used for the present calculations [16].

The rotor aerodynamic model for the Puma includes static stall, a yawed flow correction, and unsteady aerodynamic forces derived from thin airfoil theory, these forces being set to zero for stalled flow. For the swept tip, allowance is made for offsets of both the aerodynamic center and the center of gravity from the straight, undeformed elastic axis. However, the airfoil section is effectively sheared at discrete radial stations, and the vortices are considered to originate at the elastic axis.

There are three levels of wake model in CAMRAD. These are uniform inflow, nonuniform inflow with a prescribed wake geometry, and nonuniform inflow with a free wake geometry (for forward flight only). Uniform inflow here refers to an empirical model based on momentum theory that includes, for forward flight, a linear variation of the inflow over the rotor disk. The usual procedure is to begin by calculating the trimmed uniform inflow solution and then, as required, calculate the trimmed prescribed wake solution, followed by the trimmed free wake solution. The solutions presented here were obtained using the prescribed wake model. Previous calculations [17] showed little difference between the prescribed and free wakes at high advance ratio. Finite-length, straight-line vortex elements are used for the tip vortices, with an azimuth increment of 15° . The inboard wake is divided into three regions of panels

with the same azimuth increment. In the near wake, which extends azimuthally for 30° directly behind the blade, the inboard vorticity is represented by 15 panels distributed along the blade, with a greater concentration toward the tip, where the greater loading variations occur. The 15 panels in the near wake are replaced by a single panel in the far wake. Between the near and far wakes, there is an intermediate, rolling-up wake of two panels which changes with azimuth increment to represent the transition between the near and far wakes. The roll-up and far wake regions extend for a half revolution and three revolutions, respectively. By collapsing all the wake panels to finite-strength line segments, a lattice model of the rotor wake is produced. A uniform core radius (nondimensionalized by rotor radius) of 0.035 is used, of which a physically meaningful component contributes 0.015, and "lifting surface" effects not included in the "lifting line" representation contribute the remaining 0.020.

METAR.

The METAR code is a recent development at Aérospatiale and has not been described in the literature. The method is based on lifting-line theory, the blade being represented by its quarter-chord line including tip sweep and anhedral. The spanwise distribution of circulation is approximated by a step function with a trailed vortex emitted at each junction of two segments, and the timewise variation of circulation is considered as a step function with a shed vortex released at evenly distributed azimuthal stations. The wake is thus represented by a lattice composed of quadrilateral cells. The circulation over a cell is constant and is equal to that of the blade at the station and time of emission (Kelvin's theorem of vorticity conservation). The induced velocity is integrated in closed form using the Biot-Savart law for incompressible flow over linear segments. For high-speed level flight, the wake can be truncated after three revolutions without appreciable error.

The wake geometry may be prescribed by various models according to the case considered: Kocurek and Tangler's model in hover [18]; a simplified version of Egolf and Landgrebe's model [19]; or the classical undistorted wake in forward flight. The undistorted wake has proved sufficient for high-speed cruise conditions.

The airfoil characteristics are obtained from tabulated airfoil polars derived from wind-tunnel tests [20]. Compressibility effects are therefore included and power requirements, drag, and pitching moment outputs can be derived.

The Mach number, the angle of attack, and the aerodynamic chord are computed in the local reference frame attached to the quarter-chord line, which may differ from the pitch axis because of sweep or anhedral.

Various corrections may be applied to airfoil data: Reynolds correction on the drag coefficient; radial flow correction on the maximum lift coefficient and the radial skin friction; transonic extrapolation if the tables do not extend to the required Mach number; unsteady effects; and dynamic stall via the ONERA empirical model [21].

METAR is a building block which solves only for the aerodynamic loads, and it is coupled with the rigid-blade version of the Aérospatiale dynamic code R85U. METAR can produce, as an optional output, the velocity induced by the far wake only. This velocity is calculated in the same way as the complete induced velocity is, except that the cells whose centroid has not yet left a given domain about the blade are discarded from the integration.

For the correlation shown here, the main options and data used are the following:

- 25 spanwise stations (20 for Case 3)
- 36 time steps per turn (10° azimuthal increment)
- 108 wake steps (3 turns)
- undistorted wake
- NACA 0012 tables
- Reynolds number and radial flow corrections
- ONERA dynamic stall model used as a post-processor to correct $M^2 C_M$
- near wake domain: $0^\circ \leq \psi_{age} \leq 50^\circ$, where ψ_{age} is the azimuthal wake age

Four harmonics of blade flap motion and three harmonics of lead-lag motion were computed. The measured root feather motions at 2, 3, and 4 per rev were included as well, and these improved the correlation.

CAMRAD/JA Model.

The elements of the CAMRAD/JA wing and wake models relevant to the Puma calculations are described below. Features not important for this operating condition (such as blade–vortex interaction, free-wake geometry, and inboard sheet elements) are not described. A complete description of the CAMRAD/JA theory is given in Ref. 22.

The rotor aerodynamic model is based on lifting-line theory, and uses steady two-dimensional airfoil characteristics and a vortex wake. The analysis includes yawed-flow and swept-blade corrections, and unsteady aerodynamic forces from thin airfoil theory. The induced velocity is obtained from a vortex wake model.

Lifting-line theory separates the aerodynamic problem into wing and wake models, coupled by the induced velocity and the bound circulation. Guided by the results of perturbation theory, a practical implementation is as follows [23]. The outer problem consists of an incompressible vortex wake from a lifting line, with distorted wake geometry. The trailed wake arises from the bound vortex at the quarter-chord (an approximation for the second-order wing loading). The shed wake is created a quarter-chord aft of the collocation point on the wing (a lifting-line approximation for unsteady aerodynamics). The three components of induced velocity are evaluated at the wing collocation points from the wake vorticity, excluding the bound vortex. The collocation points are at the wing three-quarter-chord, in the direction of the local flow (an approximation for the second-order induced velocity). The inner problem consists of unsteady, compressible, viscous flow about an infinite-aspect-ratio, yawed wing. This wing is in a uniform flow consisting of the yawed free stream and the three components of wake-induced velocity. The inner problem is split into two-dimensional, steady, compressible, viscous flow (airfoil tables) with corrections for (1) unsteady aerodynamics (linear noncirculatory loads, but no shed wake); (2) dynamic stall; and (3) yawed flow (based on the swept wing equivalence assumption).

The utility of lifting-line theory for rotor aerodynamics comes from the use of two-dimensional, steady-airfoil tables to incorporate the effects of viscosity and compressibility in the airloading calculation. In the implementation described above, approximations to the

higher-order theory are accepted as required to retain the use of the airfoil tables. The resulting analysis is generally second-order (in the inverse of the aspect-ratio) accurate for lift, with the effects of sweep and yaw included, but it is less accurate for pitching moments.

The rotor wake model is based on a vortex lattice (straight-line segments) approximation for the wake. A small viscous core radius is used for the tip vortices. Vortex sheet elements can be used to represent the inboard wake, but here it is sufficient (and more efficient) to approximate the sheets by using line segments and a large core radius to eliminate large velocities. The wake influence coefficients are calculated for incompressible flow.

The wake rollup process is modeled. Eventually the tip vortex has the strength of the peak bound circulation at the azimuth where the wake was trailed. The possibility of there being inboard and outboard bound-circulation peaks of opposite sign is included in the rolled-up wake model. As a consequence of flap moment balance on the rotor blade, the bound circulation is negative at the blade tip in the second quadrant of the rotor disk for the high-speed cases of interest here.

An undistorted wake geometry is used, with the vortex elements convected relative to the rotor by the free stream and the mean induced velocity. Previous calculations have shown [17] that the self-induced distortions of the wake geometry have little effect for these cases.

The following are key features of the CAMRAD/JA analysis of swept-tip rotor blades:

- The lifting line (bound vortex) is at the quarter-chord, following the swept span line, with the induced-velocity collocation point at the three-quarter-chord. Note that a first-order lifting-line theory can not use a swept lifting line.
- The section Mach number used is that normal to the swept quarter-chord line. In addition, there are swept- and yawed-flow corrections for the angle of attack, which primarily affect the stall angle of attack and the drag of the blade section. However, there is no correction for the change in effective airfoil shape in swept or yawed flow.
- The aerodynamic loads are applied to the elastic blade at the quarter-chord (the airfoil table reference point), and the inertial loads are applied at the section center of gravity. For the swept tip, these points are aft of the feathering axis, and will produce elastic blade pitch and twist. However, the structural dynamics model assumes a straight elastic axis along the entire blade, so torsion and bending in the tip region is not properly represented.

The blades have a modified NACA 0012 airfoil. Since proper airfoil tables were not available, the standard NACA 0012 C81 table was used. As the actual airfoil is symmetric, the most significant errors expected are from compressibility effects on the moments. For these operating conditions, stall effects on drag and moment could also be important (on the inboard part of the blade, affecting the tip loading indirectly through the blade motion).

The calculations were performed using six flap/lag bending modes and two elastic pitch/torsion modes, 24 azimuthal stations, and 10 harmonics. The frequency of the blade fundamental pitch/torsion mode is about 5.4/4.7 per rev (for the rectangular/swept tips). The measured pitch-link loads show oscillations at around 4 per rev, suggesting that the control-system stiffness is less than the value being used.

A single rotor was analyzed, trimmed to the prescribed values of first harmonic flapping, shaft angle, and vehicle weight. Note that the same thrust is assumed for cases 1 and 2, although with the same collective the rectangular and swept-tip blades would have different

thrusts (the measured flapping does show different coning angles for the rectangular and swept-tip blades).

Airloads were calculated at 19 radial stations, with a resolution of 2% radius in the tip region. The airloads were linearly interpolated to the measurement locations at 92% and 97.8% radius. The calculated C_L is the resultant force normal to the blade chord, including the friction drag. Both the C_L and C_M include unsteady loading terms, which are particularly important for the prediction of the pitching moment.

4. LIFTING-LINE METHOD PREDICTIONS

Aircraft Trim

The four lifting-line/wake methods discussed above were run for each of the three cases using the values for vehicle weight (thrust), first harmonic flapping, and rotor-shaft angles of attack given in Table 2. The resulting collective ($\theta_{.75R}$), lateral cyclic ($-\theta_{1c}$), and longitudinal cyclic ($-\theta_{1s}$) angles are compared with the flight measurements in Table 3. There is, of course, no difference in the flight measurements for Cases 1 and 2. Note that the collective and longitudinal cyclic angles are substantially higher for Case 3 than for Cases 1 and 2, because the aircraft was in level flight in the former case and in descending flight in the latter case (5.2° flight path angle).

Table 3. Trim Control Angle Comparison

Control Angle	Case	Puma	RAE/WHL	METAR/R85U	CAMRAD	CAMRAD/JA
$\theta_{.75R}$	1	9.92	10.62	8.96	10.08	9.85
	2	9.92	9.78	9.73	9.77	9.03
	3	11.29	11.92	12.71	12.40	12.03
$-\theta_{1c}$	1	-2.41	-3.50	-3.38	-3.61	-3.68
	2	-2.41	-1.60	-2.90	-2.97	-2.90
	3	-2.10	-1.79	-4.24	-3.39	-3.35
$-\theta_{1s}$	1	9.03	8.21	6.46	7.14	7.32
	2	9.03	9.05	7.04	6.89	6.71
	3	10.04	12.59	9.12	8.68	9.09

For the analyses, no attempt was made to match the mixed-bladed rotor configuration, but instead it was assumed that there were four identical rectangular-tip blades for Case 1 and four identical swept-tip blades for Case 2. The predicted collective pitch angle for these cases is within 1° of the measurement. When the differences between the actual flight configuration and the analytical representation are considered, the differences in the control angles are not surprising. For Case 3, the analyses overestimate the collective angle by 0.6° to 1.4° despite the better correspondance between the analytical model and the flight configuration.

The variation in the lateral cyclic prediction for the three cases ranges from -2.1° to 0.8° . For the longitudinal cyclic angles, the analyses generally underestimate the measured values. These predicted values are low by as much as 2.6° , in some cases. The one exception is the RAE/WHL analysis estimate, which is 2.6° high for Case 3. The METAR/R85U code does not include a flexible torsion mode like the other analyses do, but the control angles predicted using this code do not appear to differ significantly.

Calculated Blade Airloads

The analytical models' predictions of normal force and pitching moment are compared with the flight test data in Figs. 9 to 11 for the three cases. With the exception of the RAE/WHL prediction for Case 1, these predictions are all new since the May 1988 workshop.

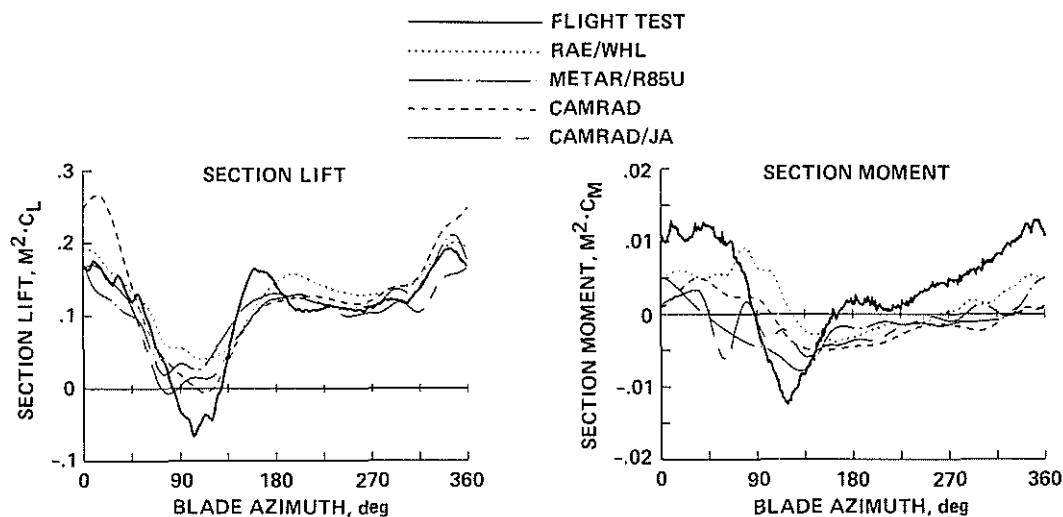


Figure 9. Comparison of lifting-line/wake methods and flight test data for Case 1 normal force and pitching moment; $r/R = 0.95$.

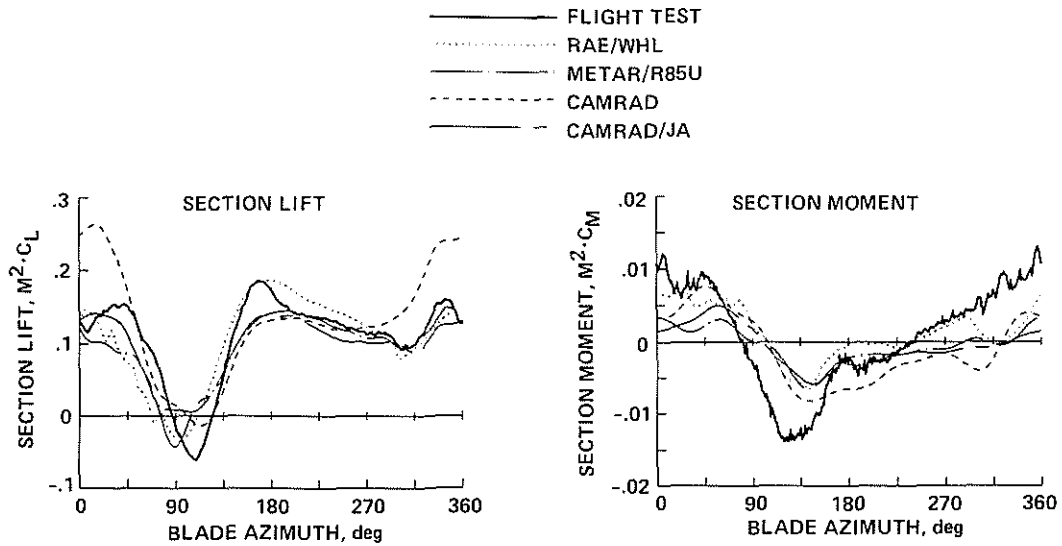


Figure 10. Comparison of lifting-line/wake methods and flight test data for Case 2 normal force and pitching moment; $r/R = 0.95$.

The various lifting-line methods agree fairly well with each other for the Case 1 normal force at $.95 R$ with the exception of CAMRAD, which shows more lift at the rear of the disk (Fig. 9). However, none of the methods show the region of negative lift that is observed at the beginning of the second quadrant, nor do they indicate the rapid rise in lift that is observed at the end of that same quadrant. There is a wide variation in the pitching moment predictions on the advancing side of the disk, and none of these predicted values match the strong positive-to-negative moment change that is observed in the data.

The agreement between the analytical predictions and the data for Case 2, shown in Fig. 10, is better than that obtained for Case 1, which is somewhat surprising considering the amount of sweep present in Case 2. The RAE/WHL and CAMRAD/JA analyses both show a substantial area of negative lift, although this negative lift leads that shown by the flight data by 15° or 20° . The prediction of the rate of lift recovery at the end of the second quadrant is also improved. The predictive capability of both of these analyses has recently been improved for swept-tip configurations by accounting for blade sweep in the evaluation of the section aerodynamic forces, and these changes have made a substantial improvement in the accuracy of the normal-force prediction. The lifting-line methods agree better with each other for the prediction of pitching moment than was seen in Case 1, and the positive-to-negative moment change on the advancing side of the rotor is similar to the measurements although neither the amplitude nor the phase is predicted well.

Figure 11 shows the lift and the pitching moment for Case 3 at three radial stations. The prediction of normal force is, in general, good. As in the other cases, CAMRAD shows too much lift over the retreating side of the disk, while METAR/R85U does not capture the area of negative lift on the advancing side very well. An examination of the pitching moment shows that all of the analyses except CAMRAD provide a good estimate of the blade moment at $.92 R$, the most inboard measurement station. However, at the more outboard stations the correlation becomes progressively worse. The measured moments become larger, whereas the lifting-line predictions show little change until $.978 R$, where some of the analyses break down.

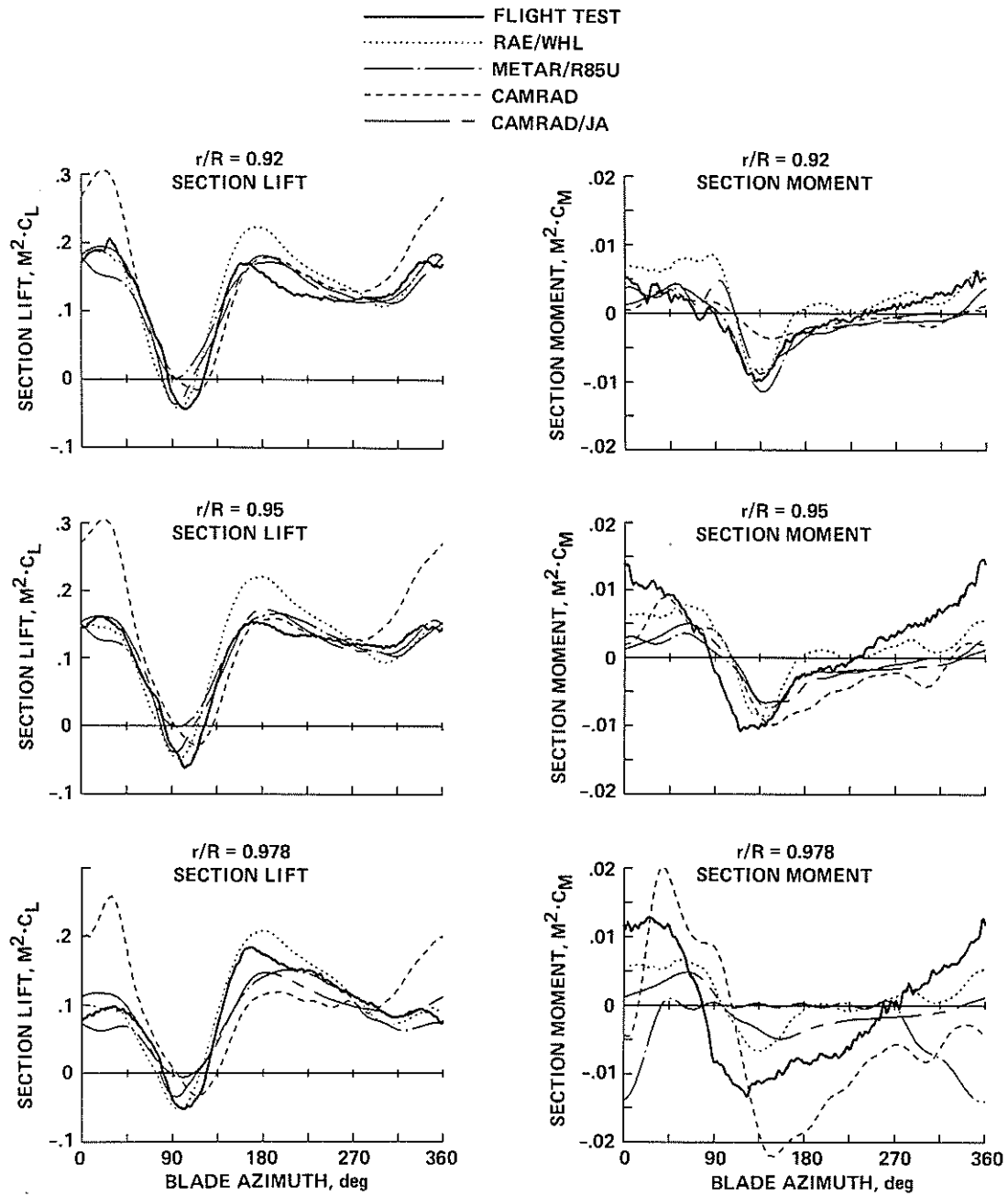


Figure 11. Comparison of lifting-line/wake methods and flight test data for Case 3 normal force and pitching moment.

The radial distribution of lift for Case 3 is shown in Fig. 12 for $\psi = 0^\circ$ and 180° . Except for CAMRAD, the analyses agree well at 0° over the outer portion of the blade, but disagree inboard where there are no measurements. At 180° , differences are seen between the predictions and the measurements. The analyses show that the lift decreases as the blade tip is approached, while the measurements show that the lift is increasing. This is characteristic of all of the Puma flight test measurements on the forward side of the disk, and is discussed in detail in the companion paper.

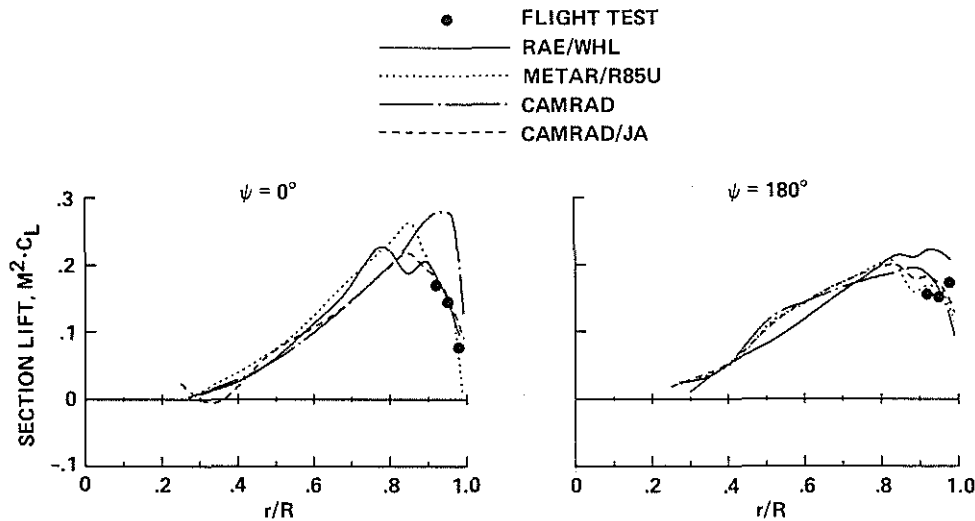


Figure 12. Comparison of lifting-line/wake methods and flight test data for Case 3 radial distribution of normal force.

5. DISCUSSION

Lifting-Line Predictions

The correlation shown here is an improvement over that obtained at the May 1988 workshop. This improvement is seen both in predictive accuracy and in agreement between the various methods. In part, this improvement is a result of minor refinements in some of the models, or slight changes in input parameters to improve consistency. A major change, however, has been made in the way that the sweep on the outer portion of the blade is modeled. Changes to the RAE/WHL analysis have resulted in a significant improvement in the prediction of the normal force for Cases 2 and 3. The predictions obtained with CAMRAD/JA also show a significant improvement over the CAMRAD predictions, as shown in Figs. 10-12. Fig. 12, in particular, shows that at the rear of the disk the differences between the two models occur primarily over the swept section. As discussed above, the major changes in the CAMRAD/JA model are the inclusion of a swept lifting line and the evaluation of the section Mach number normal to the swept quarter-chord line.

The Case 3 prediction of the pitching moment at $.92 R$ is good for all of the analyses except CAMRAD. However, the agreement degrades both in magnitude and phase at $.95 R$, and becomes poor at $.978 R$, where METAR/R85U and CAMRAD show unsatisfactory results. This behavior is in general agreement with our understanding of the limitations of lifting-line

theory for rotorcraft. Lifting-line theory can be derived formally using the method of matched asymptotic expansions where the inner problem is an infinite, yawed wing and the outer problem is the three-dimensional wake [24]. The small parameter for the expansions is the inverse of the aspect ratio. The accuracy is second-order for lift, but only first-order for moment, and therefore the moment calculation should break down before the lift calculation does as the tip is approached.

The good correlation for the Case 3 lift at $.95 R$ is not observed for the Case 2 calculations shown in Fig. 10. In particular, the region of negative lift is seen to lead the measurements by about 20° . Identical analytical models are used in both cases, and the only differences are the trim values used for harmonic flapping and shaft angle of attack. The disk-plane angle of attack is clearly different for these two cases, but the concept of a disk-plane angle of attack for the mixed-bladed rotor is not easily accepted, because each of the three blade types on that rotor is following a different track. How to improve the Case 2 correlation without developing an exact model for the mixed-bladed rotor is unclear.

The Case 1 correlation is only fair, particularly with respect to the prediction of negative lift at the start of the second quadrant. The correlation for this rectangular-tip blade is clearly poorer than that for the swept-tip blade on the opposite side of the rotor. It is not clear how to improve this correlation, because of the difficulties of modeling the mixed-bladed rotor. However, the fact that the correlation for the swept tip, with its unusual tip planform, is better than the rectangular-tip correlation is not completely satisfactory.

Flight Data

The flight test measurements have been used here as a means of judging the predictive capability of the analytical methods. However, it is also necessary to examine the flight data to determine as far as possible its reasonableness and accuracy. The availability of flight data from two separate trials of the Puma provides a limited check of the validity of the data. The same instrumented swept-tip blade was used for the initial flight trials (Case 2) and the later flight tests which employed four swept-tip blades (Case 3). Despite the fact that Cases 1 and 2 are for a descent condition, a comparison of individual pressure transducer measurements in Fig. 8 shows that the time histories are very similar. The integrated pressure distributions are also very similar except at the end of the fourth quadrant, where Case 2 shows vortex loading that is not seen in Case 3 (Fig. 6). The pitching moments at the two outboard stations are also very close, as shown in Fig. 7.

The integrated effects of the airloads and the blade dynamics are observed in measurements of the swept-tip blade's root flap angle and the pitch-link loads. Figure 13 compares these measurements for Cases 2 and 3. The flap angle comparison shows that there is substantial difference in the first harmonic flapping. The Case 2 harmonic flapping is approximately twice the Case 3 flapping and is opposite in phase (see Table 2). The coning and the higher harmonic flapping angles, however, are essentially identical for Cases 2 and 3. Some of the difference in the first harmonic flapping between Cases 2 and 3 is caused by the disk's being tilted back in the Case 2 descent condition. However, part of the difference is caused by the mixed-bladed

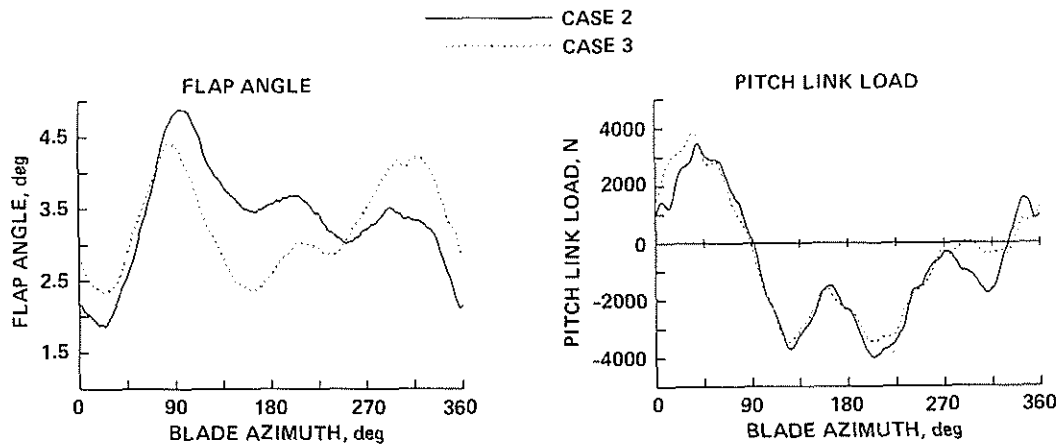


Figure 13. Comparison Cases 2 and 3 flap angles and pitch-link loads.

rotor configuration. The pitch-link loads for the two cases show very good agreement, with a slight difference seen in the fourth quadrant.

Although the results are not shown here, the accuracy of the pressure integration in the presence of supercritical flows and the absence of transducers on the first 10% of the lower surface has been assessed. For example, the oscillations that are seen in the first quadrant of the normal force shown in Fig. 5 for Case 1 are caused by shocks passing over individual pressure transducers. A proper accounting for the shock shape does not change the integrated forces and moments by more than the size of the oscillation band in the figure. The effect of the sparseness of the lower surface transducer locations is similarly small.

Prediction of Inflow Angles

The lifting-line/wake methods shown here can all be used as bases for the prediction of inflow angles to be used by the various CFD calculations. The fundamental premise in combining the lifting-line and CFD calculations is that the lifting-line method must be able to provide an accurate estimate of the inflow or velocity at the rotor blade caused by influences outside of the CFD computational grid, such as the inflow induced by the wakes of the other rotor blades, and the inflow or relative velocity that is caused by blade motion—motions that are not currently part of the CFD solution. In this sense the lifting-line solution is a necessary but not sufficient condition for an accurate CFD prediction of lift. If the lifting-line prediction of the rotor airloads is poor, and this is because of errors in the rotor wake model or blade dynamic motions, then the CFD prediction will also be poor. However, if the accuracy of the lifting-line prediction is limited by three-dimensional tip effects or by unsteady transonic flow effects, then these can be corrected in the CFD solution.

The calculation of the prescribed inflow angles required by the CFD methods is examined here using the CAMRAD/JA lifting-line/wake solution. In addition, the measured normal-force data are used to estimate or derive a quasi-steady angle of attack based on the linear expression for lift curve slope including the Prandtl-Glauert correction.

$$\alpha(t) = \frac{\sqrt{1 - M(t)^2} C_L(t)}{2\pi}$$

where $C_L(t)$ is obtained from the pressure integration measurements and 2π is used for the lift curve slope. That this approximation is reasonable is supported by Fig. 14, in which the measured C_L at $.95R$ is plotted as a function of the local Mach number and is compared to the two-dimensional table values for lift for seven values of angle of attack. What this figure shows is that except for a small region at the highest Mach number the blade is operating in the linear regime for section lift. Thus, the formula above provides a good estimate of the quasi-steady angle of attack. However, it is noted that this does not account for unsteady aerodynamic effects.

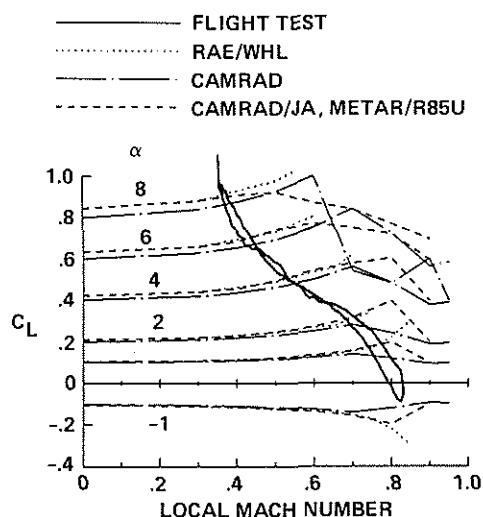


Figure 14. Comparison of measured lift as a function of local Mach number with blade tabulated lift values; Case 3, $.95R$.

Figure 15 shows various parts of the angle-of-attack calculation and compares these to the derived angle of attack. The pitch angle that is shown is the geometric angle of attack at $.95R$; it is obtained from the root feather measurement by adding in the built-in twist. This pitch angle varies from approximately 1° on the advancing side to 20° on the retreating side. The effect of inflow is to reduce the geometric pitch angle to the actual angle of attack of the blade with respect to the air. In this figure the inflow reduction is shown in two stages using the CAMRAD/JA analysis. The first stage is the angle-of-attack reduction that is caused by the far wake—that is, the flow that is induced by all the previous blades, but not the blade self-induced flow. In addition this first stage includes the angle-of-attack changes that are caused by the blade dynamic motions. The angle of attack calculated in this stage is provided to the CFD methods in the form of inflow or partial angles to account for the induced-flow terms that are outside of the computational domain. The second stage of angle-of-attack reduction is from the blade self-induced inflow and adding this results in the calculated blade angle of attack. The calculated and the derived angles of attack do not agree and, in part, the differences are due to unsteady aerodynamics that are included in the CAMRAD/JA analysis but not in the derived angle of attack. What this figure shows is that the lifting-line and CFD methods each contribute about half of the inflow. For an accurate prediction of the lift, then, it is necessary that both

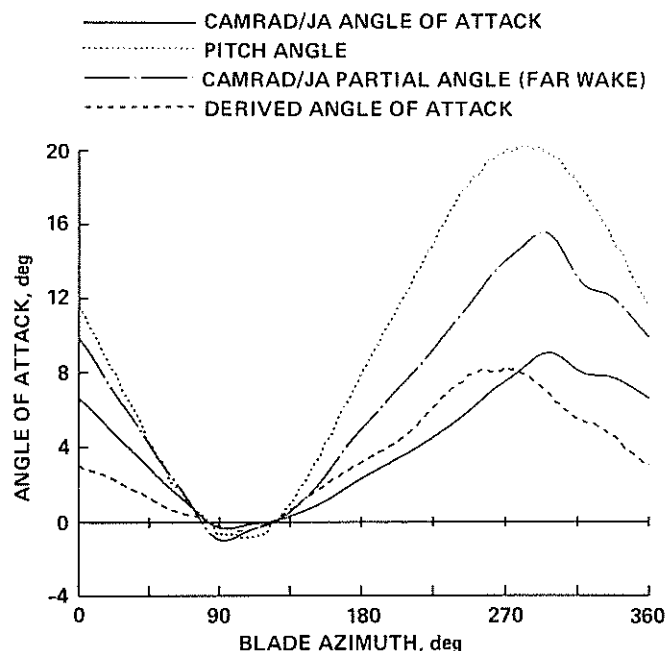


Figure 15. Terms contributing to the angle of attack for Case 3; .95 *R*.

contributions be accurate. Particularly on the advancing side, where the velocities are high, small errors in inflow can cause large differences in lift.

Progress in CFD prediction methods will require an accurate assessment of the validity of the calculations both for the lifting-line and the CFD contributions to angle of attack. As discussed here, the lifting-line method must provide the induced flows from blades outside of the computational grid as well as the inflow that is caused by blade dynamic motions. No comparisons have been shown here of measured and predicted elastic torsion motion or other blade dynamic terms that affect the angle of attack such as the $\mu\alpha_s$, $\dot{\beta}r$, and $\beta\mu \cos \psi$. Any of these terms may be sufficiently large at some azimuths to prevent the accurate prediction of lift if they are not correctly calculated. Careful work is needed in the future to isolate the reasons for correlation deficiencies.

6. CONCLUSIONS

A cooperative program has been undertaken by research organizations in the United States, England, France, and Australia to assess the strengths and weaknesses of CFD methods when compared to measurements obtained in high-speed flight. Cases have been selected from two separate trials of a research Puma with modified blades. Case 1 is measurements from a rectangular-tip blade and Case 2 is measurements from a swept-tip blade, both obtained in flight tests of a mixed-bladed rotor. Case 3 is measurements obtained on a swept-tip blade in flight trials in which all four blades had swept tips. Lifting-line/wake calculations have been made for these cases using four lifting-line methods. The conclusions of this effort with regard to the flight data and lifting-line method calculations are:

1. Flight test measurements obtained with the mixed-bladed rotor configuration (Cases 1 and 2) and the four-swept-tip-blade configuration (Case 3) are of good quality, judging

from the consistency seen between different measurement parameters and the consistency seen between the same parameters for different flight tests. These data clearly show the effects of the different tip planforms on transonic flow.

2. The lifting-line methods, in general, show good predictions of the normal force along the outer blade for Case 3. The CAMRAD model shows too much lift over the rear of the disk, which is apparently a result of the use of a straight lifting-line model (no sweep). The experimental measurements show an increase in normal force at the blade tip over the forward edge of the disk for the swept-tip blades and this effect is not captured by the lifting-line methods. The prediction of the normal force for Case 2 is not as good as that for Case 3; the difference appears to be related to the blade trim. The Case 1 predictions are poor and it is unclear whether this is a result of the unusual mixed-bladed rotor configuration or of other factors. The reasons for the poor prediction of the lift on the rectangular-tip blade cannot be determined because of unmodeled effects in the mixed-bladed rotor.
3. The lifting-line methods show good predictions of the pitching moment inboard on the blade ($.92 R$), but the predictions become poorer farther out the blade. The measurements show the pitching moment to be increasing in this region, and this increasing pitching moment appears to be the major source of the pitch-link loads.
4. The prediction of lift for rotor blades in high-speed flight depends upon accurate calculation in all stages in the process. The best of the lifting-line methods shown here are able to make accurate overall calculations in some cases. For these cases the lifting-line method can provide a solid basis for CFD calculation. It is clear that the lifting-line calculation is a necessary, but not sufficient, condition for the CFD calculation to be successful. Where the lifting-line calculation is not accurate it is unlikely that the CFD calculation will provide good information. A careful evaluation of all the links in the calculation process is required.

ACKNOWLEDGEMENT

David Fluck of the U.S. Army Aeroflightdynamics Directorate is acknowledged for his help with processing of DATAMAP files.

REFERENCES

- 1) F. X. Caradonna and W. J. McCroskey, The Development of CFD Methods for Rotor Applications, *NASA CP 2495*, March 1987, pp. 34–65.
- 2) A. Desopper, P. Lafon, P. Céroni, and J. J. Philippe, Ten Years of Rotor Flow Studies at ONERA, *Journal of the American Helicopter Society*, vol. 34, no. 1, Jan. 1989, pp. 34–41.
- 3) Roger C. Strawn and Chee Tung, Prediction of Unsteady Transonic Rotor Loads with a Full-Potential Rotor Code, *American Helicopter Society 43rd Annual Forum Proceedings*, May 1987, pp. 795–805.
- 4) R. C. Strawn and F. X. Caradonna, A Conservative Full-Potential Model for Unsteady Transonic Rotor Flows, *AIAA Journal*, vol. 25, no. 2, Feb. 1987, pp. 193-198.

- 5) Wayne Johnson, Development of a Comprehensive Analysis for Rotorcraft – I. Rotor Model and Wake Analysis, *Vertica*, vol. 5, 1981, pp. 99–130.
- 6) Wayne Johnson, Development of a Comprehensive Analysis for Rotorcraft – II. Aircraft Model, Solution Procedure and Applications, *Vertica*, vol. 5, 1981, pp. 185–216.
- 7) M. J. Riley and Judith V. Miller, Pressure Distributions on a Helicopter Swept Tip from Flight Tests and from Calculations, *Paper No. 9, Ninth European Rotorcraft Forum*, Sep. 1983.
- 8) M. J. Riley, Measurements of the Performance of a Helicopter Swept Tip Rotor in Flight, *Paper No. 35, Twelfth European Rotorcraft Forum*, Sep. 1986.
- 9) C. Young, Development of the Vortex Ring Wake Model and Its Influence on the Prediction of Rotor Loads, *AGARD Conference Proceedings No. 334*, May 1982.
- 10) J. Grant, The Prediction of Supercritical Pressure Distributions on Blade Tips of Arbitrary Shape Over a Range of Advancing Blade Azimuth Angles, *Vertica*, 3, 1979, pp. 275–292.
- 11) J. J. Chattot, Calculation of Three-Dimensional Unsteady Flow Past Helicopter Blades, *NASA TP 1721*, 1980.
- 12) R. B. Philbrick, The Data and Aeromechanics Test and Analytics Management and Analysis Package (DATAMAP) Vol I – User’s Manual and Vol II – Systems Manual, *USAAVRADCOM TR 80-D-30A and -30B*, 1980.
- 13) T. S. Beddoes, A Stall Synthesis of Unsteady Aerodynamic Effects Including Stall Hysteresis, *1st European Rotorcraft and Powered Lift Aircraft Forum*, Sep. 1975.
- 14) W. Johnson, Assessment of Aerodynamic and Dynamic Models in a Comprehensive Analysis for Rotorcraft, *Computers & Mathematics with Applications*, vol. 12A, no. 1, 1986, pp. 11-28.
- 15) C. Tung, F. X. Caradonna, D. A. Boxwell, and W. R. Johnson, The Prediction of Transonic Flows on Advancing Rotors, *American Helicopter Society 40th Annual Forum Proceedings*, May 1984, pp. 389-399.
- 16) W. Johnson, A Comprehensive Analytical Model of Rotorcraft Aerodynamics and Dynamics; Part II: User’s Manual, *NASA TM 81183*, July 1980.
- 17) Gloria K. Yamauchi, Ruth M. Heffernan, and Michel Gaubert, Correlation of SA349/2 Helicopter Flight Test Data with a Comprehensive Rotorcraft Model, *Paper No. 74, Twelfth European Rotorcraft Forum*, Sep. 1986.
- 18) J. David Kocurek and James L. Tangler, A Prescribed Wake Lifting Surface Hover Performance Analysis, *Journal of the American Helicopter Society*, vol. 22, no. 1, Jan. 1977, pp. 24-35.
- 19) T. A. Egolf and A. J. Landgrebe, Generalized Wake Geometry for a Helicopter Rotor in Forward Flight and Effect of Wake Deformation on Airloads, *American Helicopter Society 40th Annual Forum Proceedings*, May 1984, pp. 359-376.
- 20) John M. Davis, Rotorcraft Flight Simulation with Aeroelastic Rotor and Improved Aerodynamic Representation, Volume II – User’s Manual, *USAAMRDL TR 74-10B*, 1974.

- 21) C. T. Tran and D. Petot, Semi-Empirical Model for the Dynamic Stall of Airfoils In View of the Application to the Calculation of Response of a Helicopter Blade In Forward Flight, *Paper No. 48, Sixth European Rotorcraft and Powered Lift Aircraft Forum*, Sep. 1980.
- 22) Wayne Johnson, CAMRAD/JA; A Comprehensive Analytical Model of Rotorcraft Aerodynamics and Dynamics; Johnson Aeronautics Version; Volume I, Theory Manual, Johnson Aeronautics, Palo Alto, California, 1988.
- 23) Wayne Johnson, Recent Developments in Rotary-Wing Aerodynamic Theory, *AIAA Journal*, vol. 24, no. 8, Aug. 1986.
- 24) Wayne R. Johnson, Wake Model for Helicopter Rotors in High Speed Flight, *NASA CR 177507*, Nov. 1988.